the series resistance, beam divergence and resistance to degradation under high-power operation of InGaAsP-based lasers are superior to AlGaAs systems. The advantages of InGaAsP system mentioned above seem to be sufficient for replacing the AlGaAs-based lasers in present-day high-power applications, and may stimulate the search for new applications of near-infrared diode lasers. □

Received 13 December 1993; accepted 18 May 1994.

1. Endriz, J. G., *IEEE J. Quantum Electron.* **28,** 952–965 (1992).
2. Welsh, D. F., Chan, B., Streifer, W. & Scifres, D. R. *Electron. Lett.* **24,** 113–115 (1988).
3. Fukuda, M. *Reliability and Degradation of Semiconductor Lasers and LEDs* (Artech House, Boston, 1991).
4. Garbuzov, D. Z., *et al. IEEE J. Quantum Electron.* **27,** 1531–1535 (1991).
5. Razeghi, M. *InGaAsP Diodes*, U.S. Air Force Phillips laboratory, Diode laser technology program conference, Albuquerque, April 20–22 (1993).
6. Fukuda, M. *J. appl. Phys.* **59,** 4172–4176 (1986).
7. Chand, N. *Appl. Phys. Lett.* **62,** 1818–1820 (1993).
8. Diaz, J., *et al. Electron. Lett.* (Submitted).
9. Razeghi, M. *The MOCVD Challenge* (Hilger, Bristol, 1989).
10. Razeghi, M. in *Materials for Photonic Devices* (eds Andrea, A. D., Lapiccirella, A., Marletta, G. & Viticoli, S.) 15 (World Scientific, River Edge, New Jersey, 1991).
11. Dyment, J. C., *et al. Appl. Phys. Lett.* **24,** 481–484 (1974).
12. Laser Diode Product Catalog (Spectra Diode Labs, SanJose, California, 1994).
13. Larsson, A., Salzman, J., Mittelstein, M. & Yariv, A. *J. appl. Phys.* **60,** 66–68 (1986).
14. Sakamoto, M. & Kato, Y. *Appl. Phys. Lett.* **50,** 869–870 (1987).

ACKNOWLEDGEMENTS. This work is supported by the Advanced Research Projects Agency/US Army Research Office.

Density-driven liquid–liquid phase separation in the system Al_2O_3–Y_2O_3

S. Aasland* & P. F. McMillan

Department of Chemistry and Biochemistry, Arizona State University, Tempe, Arizona 85287, USA

Phase separation of liquid mixtures into two liquids with different compositions is a well-known phenomenon. It has been proposed[1–9] that another type of liquid–liquid phase separation, driven by fluctuations in density rather than in composition, may occur in some elemental systems. Transitions between low- and high-density amorphous phases have been described for the one-component oxides H_2O, SiO_2 and GeO_2 (refs 10–17), and it has been suggested[18–21] that a liquid–liquid phase transition might occur in supercooled water. If density-driven phase separation truly does occur in liquid mixtures, it should be possible to observe the coexistence of two liquids with the same composition but different density. Here we report the direct observation of such a situation. We observe two coexisting liquid phases in the supercooled melt of Al_2O_3–Y_2O_3 just above the glass transition at ambient pressure, both of which have the same composition. We propose that these two phases must differ solely in density, and that the transition is entropically driven. The occurrence of the phase transition in this system may explain why the crystallization of yttrium aluminium garnet, the host material for Nd^{3+} ions in YAG lasers, is sluggish[22–25].

The occurrence of maxima in the melting curves of many metals, alloys and simple salts has been related to the presence of distinct structural species in the liquid, with relative proportions varying with pressure and temperature[6,8]. Large changes in the electrical conductivity of molten metals and chalcogens with pressure have also been analysed by a two-species model[7,8]. Changes in the pair distribution functions of liquid Cs, Bi, Ga and Se suggest that the electrical conductivity variations are due to rapid changes in liquid structure, between low- and high-density states characterized by different coordination number and connectivity[9]. The volume change accompanying the semiconductor–metal transition in liquid Se suggests a first-order transition, implying two distinct liquid phases[2,4]. Studies on liquid S suggest transitions between three liquid phases[4]. Analysis of available data for liquid C, along with results of calculations from first principles has led to a pressure–temperature (P–T) diagram with a first-order transition between liquids with graphitic and diamond-like structures[5]. Liquid H_2O and SiO_2 both exhibit temperature maxima in their densities[26,27]. It has recently been argued for H_2O that the thermodynamic anomalies are related to critical behaviour associated with a transition between low- and high-density phases[18–21], in agreement with the observation of distinct low- and high-density forms of amorphous solid H_2O[10,28,29]. Similar arguments have been extended to SiO_2 and GeO_2 liquids and glasses, which exhibit reversible pressure-induced transitions between low- and high-density forms, associated with changes in coordination number[11–17].

The garnet $Y_3Al_5O_{12}$ (YAG) in the Y_2O_3–Al_2O_3 system is an important technological material[22–25]. Single-crystal growth of YAG is rendered difficult by its sluggish crystallization from the melt, and by the extreme temperature sensitivity of the process. In the absence of seed crystals, or if the melt temperature exceeds a 'critical' value, metastable crystallization of $YAlO_3$ perovskite and alumina occurs over a range of compositions[22–25]. Although this behaviour is primarily due to the relative growth and melting kinetics of the crystalline phases, it has sparked interest in the structural and thermodynamic properties of Y_2O_3–Al_2O_3 and related liquids[22–25,30,31].

We undertook a study of the Y_2O_3–Al_2O_3 liquid system by hot-stage microscopy. Metastable crystallization was verified near the composition of YAG, and the solidus and liquidus temperatures observed were in agreement with previous studies[22–24]. The liquids could be supercooled to several hundred degrees below the liquidus (1,300–1,400 °C). No change in the appearance of the liquid was observed while the liquid was held in this temperature regime. Glasses could be quenched from the supercooled liquid with compositions between 24–32 mol% Y_2O_3, by switching off the power to obtain a cooling rate of 300–400 degrees s^{-1}.

For all of the samples which formed glass, we observed a second liquid phase appear spontaneously throughout the bulk of the supercooled liquid sample during quenching. This second phase formed bubbles which grew during the quench, before both phases were frozen at the glass transformation temperature, T_g, giving rise to glassy inclusions in a glassy matrix (Fig. 1). Nucleation and growth of the second liquid phase were also observed at 20 and 22 mol% Y_2O_3, but these samples crystallized during quenching, and could not be obtained in the glassy state. The volume fraction of the glassy inclusion phase in the sample increased with decreasing Y_2O_3 content, and with decreasing quench rate (Fig. 1*b*, *c*), but never reached 100% for the samples which could be quenched to glass. Attempts to grow larger inclusions via slower quenching or re-heating glassy samples failed due to crystallization, which precluded calorimetric study of the glassy phases. The liquid–liquid separation temperature increased slightly but systematically with increasing Al_2O_3 content (Fig. 2). The compositions of the two glassy phases present in each sample were determined by electron probe microanalysis (Table 1). To our surprise, the glassy matrix and inclusion phases were found to have identical compositions, within experimental error ($2\sigma < \pm 2$ relative atom%), for all bulk compositions studied.

Using primary backscattered electrons to image the sample, the inclusion phase always appeared darker than the matrix, indicating a lower average electron density within the inclusion

* Present address: Department of Chemistry and Chemical Engineering, Norwegian Institute of Technology, The University of Trondheim, 7034 Trondheim-NTH, Norway.

(Fig. 1*d*). For phases with equal composition, this indicates a lower mass density for the glassy inclusions compared with their matrix. We have confirmed by optical microscopy, through observation of the direction of movement of the Becke line (the bright line of light which appears at the interface between materials of different refractive index), that the inclusions have lower refractive index than the matrix.

The lower density of the glassy inclusion phase, formed at lower temperature, gives an indication of the mechanism of the liquid–liquid transition. Because Y_2O_3–Al_2O_3 is a two-component system, 'conventional' phase separation into two liquids with different compositions might at first be invoked, with a narrow compositional gap corresponding to the small uncertainty in the electron probe analysis. However this is unlikely, because the 'unmixing' was observed to occur over a wide range of bulk compositions, and in each case gave rise to matrix and inclusion phases with identical compositions.

As an alternative approach to understand our observation, we propose the existence of a metastable liquid–liquid P–T phase boundary, between two Al_2O_3–Y_2O_3 liquids with the same composition but different density, analogous to that suggested for water[18–20] (Fig. 2). This boundary is extended into a surface in the P–T–x (where x is composition) field of the system Al_2O_3–Y_2O_3, resulting in a curve, T_{l-l}, in the constant pressure $T-x$ diagram (Fig. 2). The two liquids will coexist stably only at the phase transition temperature at a given pressure. In our quenching experiments, the higher-temperature liquid phase with higher density is retained metastably to temperatures below the coexist-

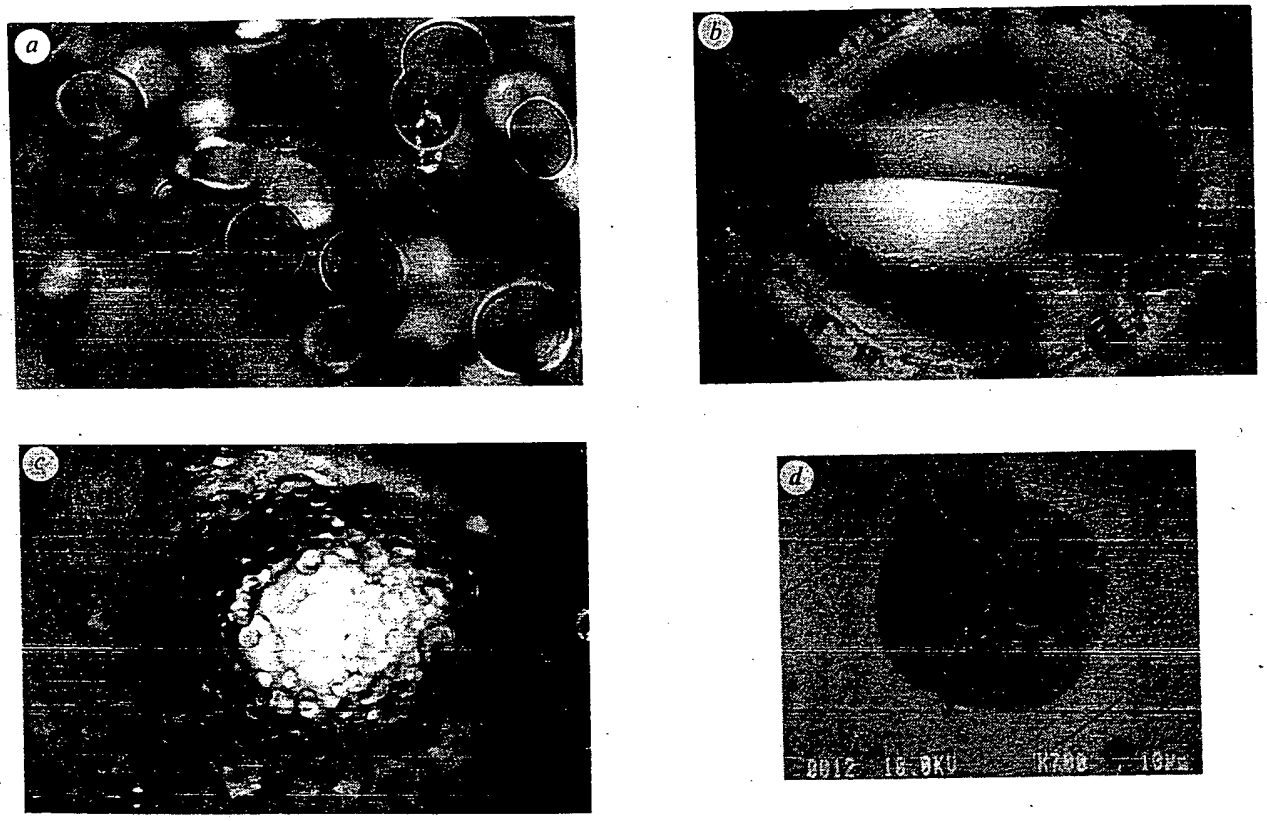

FIG. 1 *a*, Transmitted-light optical micrograph of a typical sample in the glass-forming region (30.1 mol% Y_2O_3), showing the glassy inclusion phase in a glassy matrix of the same composition. The field of view is ~100 × 150 μm. All the samples containing two glassy phases were found to be isotropic under polarized light, and no crystalline peaks were observed in the X-ray diffraction patterns (careful scans were made in the region of the strong diffraction peaks of $Y_3Al_5O_{12}$, which is the only isotropic crystalline phase in the system). Starting materials in the composition range 20–37.5 mol% Y_2O_3 were prepared by a sol–gel synthesis[34], and heated by d.c. resistance heating of a metal wire in a water-cooled microscope heating stage[35–37]. To obtain the high temperatures required for this study, the microscope hot stage[35–37] was modified by exchanging the Pt–Ir wire furnace with a pure Ir wire, operated in inert (N_2) atmosphere to avoid oxidation of the iridium. Powder samples were loaded into a 0.6-mm-diameter hole in the 1-mm-diameter Ir wire. The hot stage was placed under an optical microscope for visual examination of the samples during heating and cooling. Quenching of the liquids was achieved by rapidly turning the voltage down. Temperature was calibrated from series of known melting-point standards, including crystalline phases in the Y_2O_3–Al_2O_3 system. The temperatures at which the second liquid phase appeared, and the glass transition temperature (T_g) were estimated from the temperature at the beginning of the quench, the timed quench rate, and the calibrated power to the Ir wire furnace. *b*, *c*, Transmitted-light optical micrographs of the same glassy sample, at lower magnification than a, showing effects of variable quench rate. Both micrographs show the glassy sample in the Ir wire, which appears as the dark material (towards the corners of the micrographs) surrounding the glass. The microscope is focused just below the surface of the glass, at some depth within the hole in the Ir wire. In both photographs, the hole in the Ir furnace wire is 0.6 mm in diameter. The horizontal line in *b* (faster quench) is a cooling crack which traverses the sample. The sample in *b* was quenched rapidly from 1,900 °C, by increasing the N_2 flow rate, and switching off the power to Ir wire furnace (400 degrees s^{-1}). The inclusions in this photograph range from 5–10 μm in diameter. Micrograph *c* represents the same sample, quenched more slowly by manually turning the power down, and clearly shows growth of larger (20–50 μm diameter), more numerous glassy inclusions than in *b*. *d*, Back-scattered electron (BSE) image of a glass-in-glass inclusion in the Y_2O_3–Al_2O_3 system. The matrix is lighter (brighter BSE image) because of higher mass density at constant composition. The black areas are due to cracking in the sample. (Scale bar, 10 μm.) For all samples studied, the composition of the matrix and the inclusion were the same within the uncertainty of the probe analysis (Table 1). For the sample shown here, both the inclusion and matrix phases had Y_2O_3 contents of 30.1 ± 0.7 mol%.

TABLE 1 Analysis of quenched Y_2O_3–Al_2O_3 sample

	Glassy inclusion phase			Glassy matrix		
	Y (at%)	Al (at%)	O (at%)	Y (at%)	Al (at%)	O (at%)
	11.65	28.59	59.76	11.43	28.54	60.03
	11.69	28.59	59.72	11.54	28.30	60.16
	11.44	28.73	59.83	11.50	28.62	59.88
	11.49	28.66	59.85	11.50	28.32	60.10
	11.64	28.24	60.12	11.45	28.43	60.12
	11.42	28.51	60.07	11.39	28.37	60.24
	11.31	28.96	59.74	11.29	27.83	60.88
	11.44	28.67	59.89	11.61	28.62	59.77
	11.37	28.60	60.04	11.56	28.71	59.73
	11.61	28.11	60.29	11.46	28.26	60.28
	11.49	28.41	60.09			
	11.46	28.49	60.05			
Mean	11.50	28.55	59.95	11.47	28.40	60.12
2σ	0.22	0.42	0.34	0.18	0.48	0.31

Electron probe microanalysis of a typical Y_2O_3–Al_2O_3 glassy inclusion and surrounding glassy matrix (Fig. 1), obtained in this study. Each sample was analysed for all three elements (Y, Al and O) by wavelength-dispersive analysis, using crystalline YAG as standard. Elemental totals were 100±1% by weight. No additional elements were observed by energy-dispersive analysis. The diameter of the probe beam was of the order of 1–2 μm, much smaller than the diameter of the inclusions analysed (10–50 μm). The individual analyses in this table represent both several points within a given inclusion, and points from several different inclusions, within the same sample. The compositions of the matrix and inclusion are identical, within analytical error (reported as 2σ of the mean analysis). 10–30 points were analysed for each sample.

ence line. The lower-temperature (lower-density) liquid phase is observed to nucleate and grow within the supercooled high-density liquid matrix to form the observed inclusions, consistent with a first-order liquid–liquid transformation process. The growth rate in such processes is strongly dependent on the liquid viscosity. The measured viscosity of molten YAG shows Arrhenius behaviour[30]. Extrapolation to a glass transition in the neighbourhood of 1,150 °C gives a viscosity of 10 poise (P), rather than the necessary large value near 10^{13} P at T_g, so that the viscosity must increase rapidly in the temperature range just above T_g. It is reasonable that the liquid–liquid transformation is arrested if the transition temperature is close to T_g, and if the system is cooled rapidly through this temperature region. Attempts were made to slow the cooling rate sufficiently to allow complete transformation from the high-temperature to the low-temperature liquid phase, but this was always intersected by nucleation of crystalline phases.

We obtained micro-infrared and Raman spectra separately from the matrix (high-temperature, high-density) and inclusion (low-temperature, low-density) glassy phases (Fig. 3). The spectra of each are quite different, and show little variation with bulk composition. The spectrum of the matrix glass is quite featureless, compared with that of the glassy inclusions, which shows several broad bands (Fig. 3). This indicates that the matrix glass is more structurally disordered, that is, has a higher entropy, than the inclusion phase. Combined with the higher density of the high-temperature matrix phase, this is consistent with the negative Clapeyron slope ($dP/dT = \Delta V/\Delta S$, where ΔV and ΔS are the volume (V) and entropy (S) differences between the two liquids) proposed for the transformation (Fig. 2).

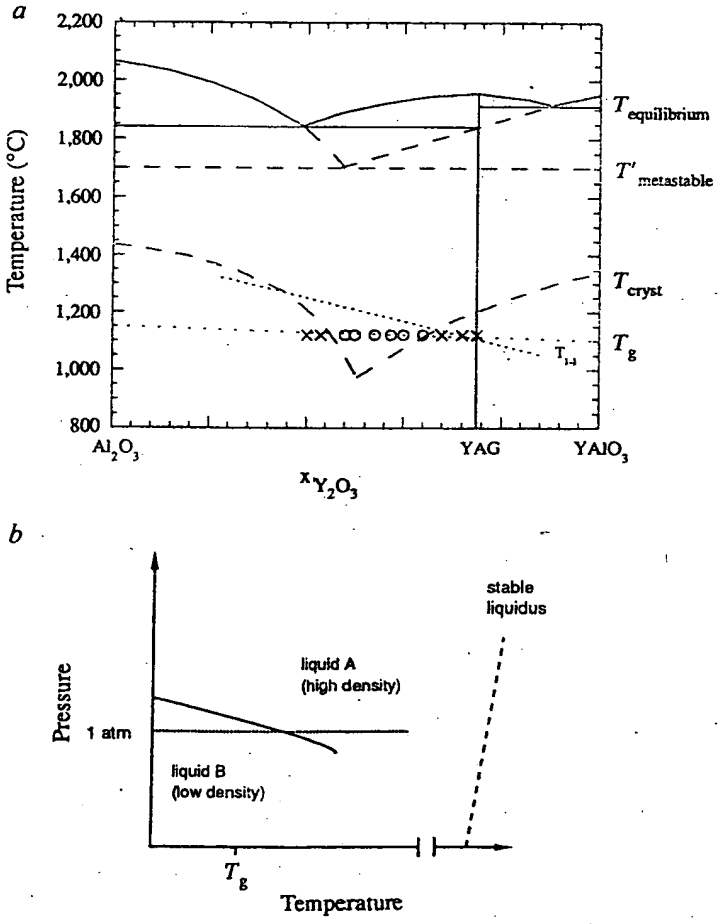

FIG. 2 *a*, The Al_2O_3–Y_2O_3 equilibrium phase diagram is shown as a solid line, together with the metastable crystallization diagram (dashed line)[22–24]. The glass-forming compositions found in this study are marked with open circles. The glass transformation temperature of the supercooled liquid (T_g) is estimated at ~1,150 °C, from optical observation of the sample freezing to glass, the temperature calibration of the furnace wire and the timed quenching rate (see Fig. 1 legend). T_g was not found to vary significantly with composition in this composition range, consistent with the relatively flat liquidus. The ratio of T_g to the melting temperature is ~2/3, consistent with many glass-forming systems[38]. Compositions which did not quench to glass are indicated by crosses. The temperatures for homogeneous or heterogeneous crystallization (T_{cryst}) in our experiments are presumed to lie sub-parallel to the metastable melting line. The intersection of T_{cryst} with T_g defines the glass-forming region in our study. A higher quenching rate, or use of containerless conditions[38–41], would extend the glass-forming region and thereby probably the region where we can find a second liquid phase. The line T_{l-l} indicates the temperature at which the second liquid phase is observed to nucleate (measured during the quench by the timed quenching rate, and the calibrated furnace power), and decreases with increasing Y_2O_3 content. Our experimental observation that the volume fraction of the low-temperature phase increases with decreasing Y_2O_3 content, also indicates that the separation between T_g and T_{l-l} increases with decreasing Y_2O_3 content. *b*, The proposed metastable liquid–liquid transformation line in the P–T plane (at fixed composition within the Y_2O_3–Al_2O_3 system), drawn by analogy with the suggested phase behaviour of supercooled liquid water[18–21], which gives a thermodynamic rationalization for our experimental result. The two liquids have the same composition, but different densities. The high-temperature liquid, corresponding to the glassy matrix phase in Fig. 1, has higher density than the low-temperature liquid which gives rise to the glassy inclusions. The high-temperature, high-density (matrix) liquid also has higher entropy (Fig. 3), so that the Clapeyron slope ($dP/dT = \Delta V/\Delta S$) is negative. The observed liquid–liquid phase separation is quite likely to be general for such A_2X_3 systems. In our case, it was fortunate that the liquid–liquid coexistence line intersected our cooling line (dotted) above T_g (and above the critical temperature for crystallization) at room pressure, so that it could be observed and the samples quenched to glass in our experiments.

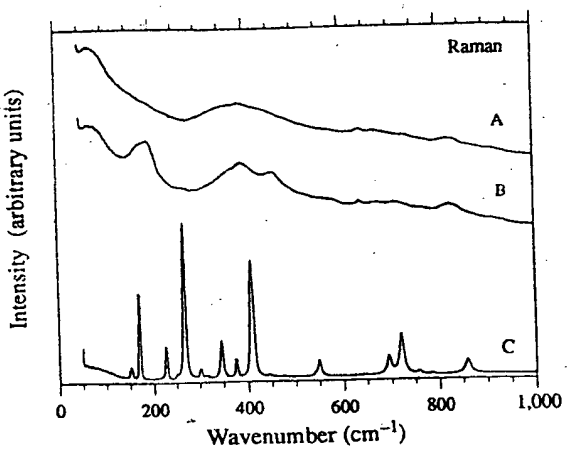

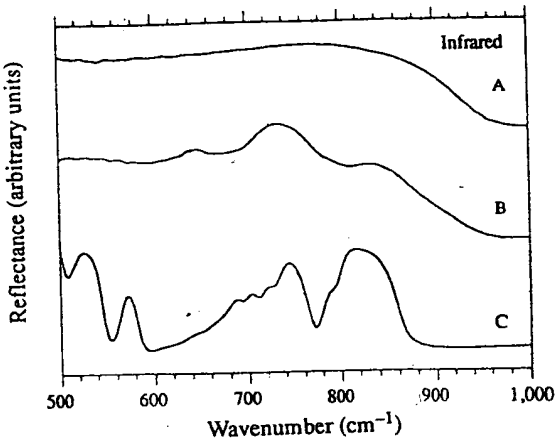

FIG. 3 Raman (left) and infrared (right) spectra of the glassy matrix (A) and glassy inclusion (B) phases from a typical sample, together with the spectra of single crystal YAG[42,43] (C). The spectra of the glassy compounds are clearly different from the spectrum of single-crystal YAG, confirming that the inclusions are not crystalline YAG, which is the only optically isotropic crystalline phase in the system. The infrared and Raman spectra of the inclusion contain more structure than the matrix, indicating that a structural change to a more ordered liquid has taken place. There are only minor changes in the vibrational spectra of the glassy inclusion and matrix phases with composition, over the range studied.

We can generally relate the liquid density behaviour to structural changes in the solid state. Crystalline YAG has been shown to decompose to $YAlO_3$ and Al_2O_3 at pressures around 40 kbar at 1,000 °C (ref. 32). The four-coordinated Al^{3+} ions in the garnet change to six-coordination, in $YAlO_3$ and Al_2O_3, and the overall density is increased. If the supercooled liquid is examined at constant temperature (Fig. 2), the lower-density liquid probably has a smaller average Al coordination than the high-density liquid phase, by analogy with the crystalline phase transition.

A structural interpretation for the thermal liquid–liquid transformation can be gained by considering the oxygen environments in corresponding crystals. In the garnet crystal, the O^{2-} ions all have the same coordination environment (OY_2Al_2). In crystalline $YAlO_3$ and Al_2O_3, several different O^{2-} environments are encountered (OAl_4, OY_3Al_2, OY_2Al_2)[33]. If the low-temperature liquid, like crystalline YAG, has a small number of distinct oxygen environments, it will have lower entropy than a high-temperature liquid with a greater range of oxygen sites.

This observation could help explain the sluggish crystallization of YAG, with a structural requirement of a single type of oxygen site, from the high-temperature melt, which corresponds to the high-entropy liquid phase. In addition, because crystalline YAG melts to the high-entropy liquid, the resulting large $-T\Delta S$ term associated with melting could be responsible for depressing the YAG liquidus, which is nearly flat in the region of the garnet composition[22–24]. □

Received 23 December 1993; accepted 6 May 1994.

1. Ferraz, A. & March, N. H. *Phys. Chem. Liq.* **8,** 289–298 (1979).
2. Brazhkin, V. V., Voloshin, R. N. & Popova, S. V. *Zh. eksp. teor. Fiz.* **50,** 392–395 (1989).
3. Brazhkin, V. V., Popova, S. V., Voloshin, R. N. & Umnov, A. G. *High. Press. Res.* **6,** 363–369 (1991).
4. Brazhkin, V. V., Voloshin, R. N., Popova, S. V. & Umnov, A. G. *Phys. Lett.* **A154,** 413–415 (1991).
5. van Thiel, M. & Ree, F. H. *Phys. Rev.* **B48,** 3591–3599 (1993).
6. Rapoport, E. *J. chem. Phys.* **46,** 2891–2895 (1967).
7. Rapoport, E. *J. chem. Phys.* **48,** 1433–1437 (1968).
8. Endo, H., Tamura, K. & Yao, M. *Can. J. Phys.* **65,** 266–285 (1987).
9. Tsuji, K. *J. non-cryst. Solids* **117/118** 27–34 (1990).
10. Mishima, O., Calvert, L. D. & Whalley, E. *Nature* **314,** 76–78 (1985)
11. Gibbons, R. V. & Ahrens, T. J. *J. geophys. Res.* **76,** 5489–5498 (1971).
12. Sugiura, H., Kondo, K.-I. & Sawaoka, A. in *High-Pressure Research in Geophysics* (eds Akimoto, S. & Manghnani, M. H.) 551–561 (Reidel, Dordrecht, 1982).
13. Grimsditch, M. *Phys. Rev. Lett.* **52,** 2379–2381 (1984).
14. Hemley, R. J., Mao, H. K., Bell, P. M. & Mysen, B. O. *Phys. Rev. Lett.* **57,** 747–750 (1986).
15. Williams, Q. & Jeanloz, R. *Science* **239,** 902–905 (1988).
16. Itie, J. P. *et al. Phys. Rev. Lett.* **63,** 398–401 (1989).
17. Smith, K. H., Chizmeshya, A. V. G. & Wolf, G. H. *EOS* **74,** 630 (1993).
18. Poole, P. H., Scortino, F., Essmann, U. & Stanley, H. E. *Nature* **360,** 324–328 (1992).
19. Poole, P. H., Essmann, U., Scortino, F. & Stanley, H. E. *Phys. Rev.* **E48,** 4605–4610 (1993).
20. Poole, P. H., Scortino, F., Essmann, U. & Stanley, H. E. *Phys. Rev.* **E48,** 3799–3817 (1993).
21. Angell, C. A. *J. phys. Chem.* **97,** 6339–6341 (1993).
22. Cockayne, B. & Lent, B. *J. cryst. Growth* **46,** 371–378 (1979).
23. Castavsky, J. L. & Viechnicki, D. *J. J. mater. Sci.* **15,** 1709–1718 (1980).
24. Gervais, M., Le Floch, S., Rifflet, J. C., Coutures, J. & Coutures, J. P. *J. Am. Ceram. Soc.* **75,** 3166–3168 (1992).
25. Nicolas, J., Coutures, J., Coutures, J. P. & Boudot, B. *J. Solid St. Chem.* **52,** 101–113 (1984).
26. Brückner, R. *J. non-cryst. Solids* **5,** 123–175 (1970).
27. Angell, C. A. & Kanno, H. *Science* **193,** 1121–1122 (1976).
28. Burton, E. F. & Oliver, W. F. *Nature* **135,** 505–506 (1935).
29. Bellissent-Funel, J. & Feixeira, J. *J. chem. Phys.* **87,** 2231–2235 (1987).
30. Fratello, V. J. & Brandle, C. D. *J. cryst. Growth* **128,** 1006–1010 (1993).
31. Voron'ko, Y. K. *et al. Soviet Phys. Dokl.* **32,** 61–64 (1988).
32. Merezio, M., Remeika, J. P. & Jayaraman, A. *J. chem. Phys.* **45,** 1821–1824 (1966).
33. Wells, A. F. *Structural Inorganic Chemistry* (Clarendon, Oxford, 1984).
34. Douy, A. & Odier, P. *Mater. Res. Bull.* **24,** 1119–1126 (1989).
35. Richet, P. *et al. J. appl. Phys.* **74,** 5451–5456 (1993).
36. McMillan, P. F., Poe, B. T., Gillet, P. & Reynard, B. *Geochim. cosmochim. Acta* (in the press).
37. Poe, B. T., McMillan, P. F., Coté, B., Massiot, D. & Coutures, J. P. *J. Am. Ceram. Soc.* (in the press).
38. Zarzycki, J. *Les Verres et l'Etat Vitreux* (Masson, Paris, 1982).
39. Coutures, J. P., Berjoan, R., Benezech, G., & Granier, B. *Revue. int. Hautes Temp. Réfractaires* **15,** 103–114 (1978).
40. Badets, M. C., Coté, B., Simon, P. & Coutures, J. P. *Ann. Chim. Fr.* **15,** 455–461 (1990).
41. Nordine, P. & Atkins, R. M. *Rev. Sci. Instrumen.* **53,** 1456–1464 (1982).
42. Hurrell, J. P., Porto, S. P. S., Chang, I. F., Mitra, S. S. & Bauman, R. P. *Phys. Rev.* **173,** 851–856 (1968).
43. Hofmeister, A. M. & Campbell, K. R. *J. appl. Phys.* **72,** 638–645 (1992).

ACKNOWLEDGEMENTS. This study was initiated after discussing YAG crystallization behaviour with J. P. Coutures and co-workers. We thank P. Poole for discussion and T. Grande for advice and for help with electron microprobe analysis. This work was supported by a grant from the US NSF to P.F.M.